

Elastic Shape Analysis of Movement Data

J.E. Borgert^{1,2}, Jan Hannig¹, J.D. Tucker³, Liubov Arbeeva², Ashley N. Buck^{2,4,5},
Yvonne M. Golightly^{2,6,7}, Stephen P. Messier⁸,
Amanda E. Nelson^{2,7,9}, J.S. Marron¹

¹Department of Statistics & Operations Research, University of North Carolina, Chapel Hill, NC

²Thurston Arthritis Research Center, University of North Carolina, Chapel Hill, NC

³Statistical Sciences, Sandia National Laboratories, Albuquerque, NM

⁴Human Movement Science Curriculum, University of North Carolina, Chapel Hill, NC

⁵Department of Exercise & Sport Science, University of North Carolina, Chapel Hill, NC

⁶College of Allied Health Professions, University of Nebraska Medical Center, Omaha, NE

⁷Department of Epidemiology, Gillings School of Global Public Health, University of North Carolina, Chapel Hill, NC

⁸Department of Health & Exercise Science, Wake Forest University, Winston-Salem, NC

⁹Department of Medicine, University of North Carolina, Chapel Hill, NC

Abstract

Osteoarthritis (OA) is a prevalent degenerative joint disease, with the knee being the most commonly affected joint. Modern studies of knee joint injury and OA often measure biomechanical variables, particularly forces exerted during walking. However, the relationship among gait patterns, clinical profiles, and OA disease remains poorly understood. These biomechanical forces are typically represented as curves over time, but until recently, studies have relied on discrete values (or *landmarks*) to summarize these curves. This work aims to demonstrate the added value of analyzing full movement curves over conventional discrete summaries. Using data from the Intensive Diet and Exercise for Arthritis (IDEA) study ([Messier et al., 2009, 2013](#)), we developed a shape-based representation of variation in the full biomechanical curves. Compared to conventional discrete summaries, our approach yields more powerful predictors of disease severity and relevant clinical traits, as demonstrated by a nested model comparison. Notably, our work is among the first to use movement curves to predict disease measures and to quantitatively evaluate the added value of analyzing full movement curves over conventional discrete summaries.

Keywords: Functional data analysis, Ground reaction forces, Human movement data, Object oriented data analysis, Osteoarthritis, Shape statistics

1 Introduction

Osteoarthritis (OA) is a prevalent degenerative joint disease characterized by cartilage loss, bone and soft tissue changes, joint pain, and diminished function. In the United States, OA affects at least 19% of adults aged 45 years and older, with the knee being the most frequently affected joint, accounting for more than 80% of the total burden of the disease (Dillon et al., 2006; Jordan et al., 2007; Lawrence et al., 2008; Vos et al., 2012). Knee OA is characterized by both the severity of radiographic damage and clinical symptoms, such as in knee pain and function. Previous research, such as in Zhang and Jordan (2010), indicated that risk factors and disease progression may vary by clinical phenotype. Additionally, important work like Felson (2013) and Guilak (2011) identified biomechanical factors in the etiology and pathogenesis of knee OA.

Biomechanical variables, particularly forces exerted during walking, are often measured in modern studies of joint injury and OA. However, the relationship among gait patterns, clinical profiles, and OA disease remains poorly understood. Biomechanical forces, collected continuously during gait analysis, are typically represented as curves over time. Discrete summaries, such as peak values, are commonly used to analyze patterns in *joint loading* (forces acting on the knee joint). Such discrete summaries are called *landmarks* in the shape statistics terminology of Dryden and Mardia (2016). Analyses based on conventional discrete summaries, such as those by Sims et al. (2009) and Astephen et al. (2008), have identified differences between groups (e.g., sex differences) and indicated variations in gait patterns which contribute to knee OA-related outcomes. Recent work by Buck et al. (2024) evaluated the ability of various clinical traits and conventional discrete summaries of gait forces to predict early symptomatic knee OA. While simplifying the statistical methods required for analysis, relying on conventional discrete summaries risks overlooking

information encoded in the complete range and patterns of movement data. Research by [Muniz et al. \(2006\)](#), [Costello et al. \(2021\)](#), [Bjornsen et al. \(2024\)](#), [Davis et al. \(2019\)](#), and others has demonstrated the value of analyzing full movement curves. However, these studies are limited and have not been formally compared to analyses based on conventional discrete summaries. For harmonic analyses of full movement curves, see [Trentadue and Schmitt \(2024\)](#) and references therein.

The primary goal of this work is to demonstrate the value added from analyzing full movement curves over conventional discrete summaries. We take an Object Oriented Data Analysis (OODA) approach for this analysis. OODA, described in [Marron and Dryden \(2021\)](#), is a framework for interdisciplinary research that introduces new terminology and methodologies for analyzing complex data. It emphasizes the careful selection of relevant data objects and the utilization of methods intrinsic to the corresponding object spaces. This approach enables the consideration of full movement data curves as complex data objects in high-dimensional space. Furthermore, the richer information within these curves presents numerous choices for both the *data object* of interest and the appropriate methodology for analysis.

Using data from the Intensive Diet and Exercise for Arthritis (IDEA) study ([Messier et al., 2009, 2013](#)), we developed a shape-based representation of variation in the full biomechanical curves. Our approach, compared to conventional discrete summaries, yields more powerful predictors of disease severity and relevant clinical traits, as demonstrated by a nested model comparison. Notably, our work is among the first to use movement curves to predict disease severity and to quantitatively evaluate the added value of utilizing full movement curves as predictors over conventional discrete summaries.

2 Curves as data objects

For the IDEA study, participants wore laboratory-provided cushioned shoes and walked at their preferred speed on a 22.5m walkway. Kinetic data, including Ground Reaction Force (GRF), were collected using an Advanced Medical Technologies, Inc. model OR-6-5-1 force plate (480 Hz) and filtered using a 4th order low-pass Butterworth filter with a cutoff frequency of 6 Hz. The GRF consists of three components: vertical GRF (vGRF), representing the force exerted downwards; anterior-posterior GRF (apGRF), the propulsive or braking force in the direction of walking; and medial-lateral GRF (mlGRF) in the third orthogonal direction.

When plotted as a function of time, the horizontal axis reflects the percentage of *stance* (time interval of foot contact with the ground) over a gait cycle with body weight-normalized force values (measured in Newtons) on the vertical axis.

Successful walking trials required the entire foot to be on the force plate during the stance phase, with participants maintaining their preferred walking speed within $\pm 3.5\%$. Walking speed was defined as the mean speed over six practice trials, during which participants walked a 10m walkway at a self-selected, stable, and comfortable pace. A photocell system registered the speed, providing immediate visual feedback.

We studied the part of the IDEA data that contained measurements of each GRF component taken at a constant sampling rate over the duration of each step. For each IDEA participant, three trials per limb were collected. For some participants, one or more trials were missing from the data. In those cases, we used as many trials as were given in the data and did not impute. We considered the collection of all trials of both limbs of all participants.

The complete set of curves for each GRF component contained 2686 curves from 454

participants. The top left panel of Figure 1 shows the collection of raw data vGRF curves colored by walking speed. There, the rainbow descends from fastest walking speed (red) to slowest (purple). Notice that many of those curves have consecutive starting and trailing zeros, which are outside the stance phase (i.e., after the foot has left contact with the force plate, but force data were still being collected) and hence do not correspond to a meaningful part of the measurements. Consequently, we define the beginning of the force curve as the zero value immediately preceding the first nonzero value, and similarly, the end of the curve as the zero value immediately following the last nonzero value. To establish a common time axis across all curves, we utilized the relevant segment of each curve and re-scaled the horizontal axis (time axis) to the unit interval $[0,1]$. Additionally, we applied linear interpolation to the force values, aligning them to an evenly spaced grid. Time normalization to the stance phase (0–100%) is a standard approach in biomechanics for analyzing GRFs and other kinetic variables, as it allows for a focus on differences in loading patterns, which is central to understanding the biomechanics of knee OA. The most commonly used method for this is *linear length normalization*, which rescales the time axis so that all stance phases are standardized to the same duration (Helwig et al., 2011), as applied in our analysis. While this approach removes explicit information about stance duration, it retains temporal differences in key gait events in the loading pattern, such as peaks and valleys, which are more relevant for understanding knee OA. In this work, we choose to focus on a careful analysis of shape, leaving the inclusion of stance duration in the analysis as a direction for future work. However, stance duration is strongly correlated with walking speed and distance (Hebenstreit et al., 2015), which were retained as clinical variables considered in our analysis.

The top right panel of Figure 1 presents the collection of vGRF curves shown in the

first panel, following this processing. Those curves are also color-coded according to their respective walking speeds. Similar results were achieved using the same processing steps for the apGRF and mlGRF curves, and are shown in the bottom left and bottom right panels of Figure 1, respectively. For a more detailed view of GRF curve variations across walking speeds, additional plots showing subsets of the curves grouped by deciles of walking speed are provided in Section 1 of the supplementary material.

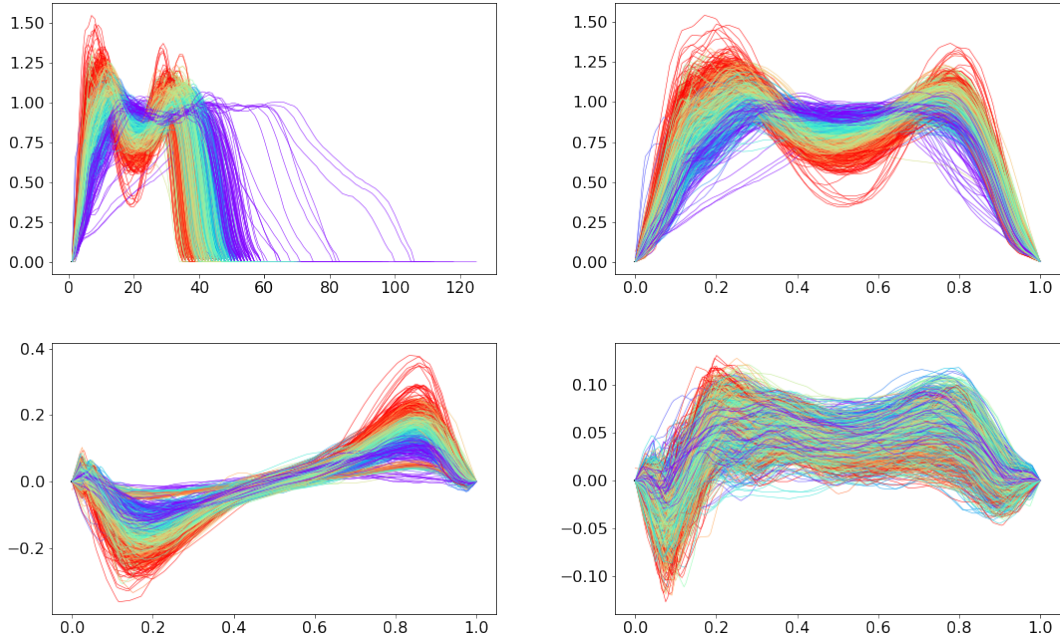


Figure 1: Top left panel: Raw vertical ground reaction force (vGRF) curves before processing, colored by walking speed. Top right: The same curves after re-scaling and interpolation of the time axis. The common rainbow color palette descends from fastest walking speed (red) to slowest (purple). Bottom row panels show apGRF curves (left) and mlGRF curves (right) after the same processing of the time axis. Note that the vertical axis (measured in N/kg, i.e. percentage of body weight) of each panel is scaled to the data it displays.

2.1 Conventional discrete summaries

Most relevant studies of GRF data, such as those in [Messier et al. \(1992\)](#), [Hunt et al. \(2006\)](#), [Zeni Jr and Higginson \(2009\)](#), and [Wiik et al. \(2017\)](#), focus on discrete summaries (also called landmarks) rather than analyzing the full curves. These discrete summaries typically correspond to critical subphases of stance during gait, such as the first and second vGRF peaks (heel-strike and toe-off) and positive and negative peaks of the apGRF curve (braking and propulsion). In contrast, mlGRF curves are highly variable and therefore more challenging to interpret and summarize ([Costello et al., 2021](#)). Consequently, GRF studies primarily analyze only the vGRF and apGRF directions.

Traditionally, greater attention has been given to the first vGRF peak, as heel-strike is a primary indicator of compressive joint loads and has been consistently linked to knee OA onset and progression. However, recent work by [Buck et al. \(2024\)](#) (and references therein) indicated that the valley (reflecting mid-stance) and the second peak of the vGRF curve are better predictors of knee OA-related symptoms.

In this analysis, we focus on three conventional discrete summaries: (1) the first vGRF peak, (2) the apGRF braking peak, and (3) the apGRF propulsion peak. Throughout the remainder of this paper, we refer to the 3-dimensional vector containing these landmark values as the *conventional discrete summary predictors*. While other landmark choices could have been analyzed, as discussed in the preceding paragraphs, these three were selected because they are the most commonly studied GRF features in biomechanical research on knee OA.

The first vGRF peak is defined in the references aforementioned as the maximum value within the first 50% (0-50%, heel-strike to midstance) of the stance phase (0-50%) (0-0.5 on the horizontal axis in Figure 1). Similarly, the apGRF braking peak is defined as the

minimum value over the first 50% of the stance phase, and the apGRF propulsion peak is defined as the maximum value over the second 50% (50 – 100%, mid-stance to toe-off) of the stance phase (0.5-1.0 on the horizontal axis in Figure 1).

3 Shape-based functional data analysis

3.1 Elastic shape analysis

The goal of our analysis was to characterize patterns of variation in gait using information in the full force curves. Many datasets of curve data have variation that appears to be either vertical or horizontal in nature. This variation is termed *amplitude* and *phase* variation, respectively. In this context, horizontal variation is viewed as a potentially important aspect of gait, while in other contexts it may represent temporal misalignment. The curves shown in Figure 1 exhibit interesting variation of both types. In particular, there is clear phase variation in the timing of the vGRF and mlGRF peaks, as well as the shift from posterior to anterior force in the apGRF curves.

Elastic warping of the time axis can provide aligned curves that better capture amplitude variation, as studied in Section 2.1 of Marron and Dryden (2021). This is important because poor alignment of curves due to phase variation can impact statistical methodology, potentially obscuring important geometric structure. As noted by Helwig et al. (2011), temporal alignment is a critical consideration in gait analysis, with various approaches being applied in gait studies. That paper highlights that while linear length normalization, which we applied as a pre-processing step, removes differences in stance duration, it does not account for phase variation in the timing of key events (e.g., peaks and valleys). Other methods discussed by Helwig et al. (2011) require extensive manual tuning and may in-

introduce distortions in curve shape. The results discussed in that paper provide evidence for the need for an alignment method that captures phase variation while preserving curve shape and minimizes manual tuning.

Elastic warping involves a transformation of the time axis, which is described by a curve that can be usefully thought of as a stretching and compression of the horizontal axis. The functions are aligned by finding the *Karcher mean* (Tucker et al., 2013) which produces aligned functions and warping functions and will be defined later on. A warping function: $\gamma(x) : [0, 1] \rightarrow [0, 1]$ is strictly increasing, invertible, and *diffeomorphic*, in other words the function and its inverse are smooth. The collection of such warping functions serve as *phase* data objects.

Aligning points across functions is often referred to as *registration*. Many conventional Functional Data Analysis (FDA) techniques rely on the \mathbb{L}^2 norm, which simplifies computations into point-wise evaluations. While point-wise computations involve *vertical registration*, other methods focus on the *shape* of functions. L^2 -based methods present well-known challenges, as detailed in Marron et al. (2015). *Elastic shape analysis*, as proposed in Srivastava et al. (2011); Tucker et al. (2013), uses the warp-invariant Fisher-Rao metric to overcome the limitations of conventional \mathbb{L}^2 -based alignment techniques. This framework dates back to such seminal work as Younes (1998) and is the first to enable fully automatic (meaning that no manual tuning is needed) shape-based registration. For each curve, the elastic shape analysis method computes the warp needed to align its peaks to a template mean curve, known as the Karcher mean. The Karcher mean is the curve that lies in the “center” of all the warped curves, and it minimizes the total distance (under the Fisher-Rao metric) between itself and all the aligned curves.

The key idea of this method is to define an equivalence relation between curves. *Am-*

plitude (or called *shape* in [Srivastava et al. \(2011\)](#); [Wu et al. \(2024\)](#)) of the data objects are equivalence classes. Two curves $f_1(x)$ and $f_2(x)$ are called equivalent, $f_1 \sim f_2$, if there exists a warping function γ such that $f_1(\gamma(x)) = f_1 \circ \gamma(x) = f_2(x)$. Then, the set of all warps of a function f , given by

$$[f] = \{f \circ \gamma : \gamma \in \Gamma\},$$

is the amplitude equivalence class.

The Fisher-Rao metric defines a proper distance on the set of such equivalence classes. In the elastic shape analysis framework, a *Square Root Velocity Function* (SRVF) representation transforms the Fisher-Rao metric into the standard \mathbb{L}^2 metric, allowing for a natural framework for the computations required for curve alignment. The Karcher mean equivalence class is defined using this distance, along with the warping functions needed to align individual functions to the Karcher mean template. The SRVF of a function $f \in \mathcal{F}$ is given by $q(t) = \text{sign}(\dot{f}(t))\sqrt{|\dot{f}(t)|}$. For any time warping of f by $\gamma \in \Gamma$, the SRVF of the warped function is given by $(q \circ \gamma)\sqrt{\dot{\gamma}}$, which we will denote by $q \star \gamma$ for convenience. Then, the warping functions needed to align a collection of curves f_1, \dots, f_n with corresponding SRVF representations, q_1, \dots, q_n , to the Karcher mean μ_q^* are computed by solving the optimization problem:

$$\mu_q^* = \arg \min_{q \in \mathbb{L}^2} \sum_{i=1}^n \left(\inf_{\gamma \in \Gamma} \|q - q_i \star \gamma\|^2 \right).$$

The output of this optimization problem is the Karcher mean μ_q^* and the set of optimal warping functions $\{\gamma_i^*\}$, and the problem is solved using *dynamic programming*. To implement this, the time domain $[0, 1]$ is discretized into N equally spaced bins, and each warping function γ_i is approximated by a piecewise linear mapping from $(0, 0)$ to $(1, 1)$. This discretization corresponds to a path through an $N \times N$ grid, where each step must have a positive slope to ensure invertibility.

In our analysis, we found substantial benefits by penalizing the amount of elasticity in the alignment of the curve. This is achieved by modifying the optimization problem to include a penalty term on the roughness of the γ_i as follows:

$$\mu_q^* = \arg \min_{q \in \mathbb{L}^2} \sum_{i=1}^n \left(\inf_{\gamma \in \Gamma} \|q - q_i \star \gamma_i\|^2 + \lambda \mathcal{R}(\gamma_i) \right)$$

The penalty $\mathcal{R}(\gamma_i)$, controlled by the constant $\lambda > 0$, imposes a constraint on γ_i . In our approach, we restrict the second derivative of γ_i , where $\mathcal{R}(\gamma_i) = \int_0^1 \ddot{\gamma}_i(t) dt$. This places a restriction on the smoothness in γ_i and has the effect of keeping γ_i closer to the identity warp $\gamma_i(t) = t$, thus regulating the level of elasticity in the alignment. The case $\lambda = 0$ is referred to as *fully elastic alignment*, while $\lambda = \infty$ is non-elastic.

The penalty is computed along the grid path and incorporated into the total cost, which is then minimized using dynamic programming in the same manner as without the penalty. This approach is similar to the method described by Wu and Srivastava (2011), where further details on the algorithm are provided.

An interesting alternative to adding a smoothness penalty is a metric learning approach that considers the broader 1-parameter family of elastic metrics, which extends SRVFs as described in Bauer et al. (2024). This family allows for flexible control over warping by varying the transformation in the metric, thereby implicitly enforcing smoothness without requiring an additional penalty term on the γ_i .

For an intuitive overview of the elastic shape analysis procedure and a more detailed derivation of the Karcher mean, see Section 9.1.3 of Marron and Dryden (2021). A thorough comparison of functional data analysis with and without phase-amplitude separation is provided in Chapters 2.1, 5.4, and 9 of Marron and Dryden (2021), demonstrating its importance for data exhibiting both types of variation. Given these established results, the observed phase variation in the GRF data motivated our application of elastic shape

analysis, from which we obtained a decomposition into amplitude and phase data objects. The following subsection details our implementation and selection of the penalty parameter λ .

3.1.1 Implementation and penalty parameter selection

The elastic shape analysis procedure was implemented via the FDASRSF Python package (Tucker et al., 2013). One possible approach to registering the GRF curve data is to apply the elastic shape alignment to each GRF component (vGRF, apGRF, mlGRF) separately. An analysis of amplitude and phase using this component-wise registration in the IDEA study data is detailed in Section 4.4 of Xiang (2023). However, that approach is less meaningful kinetically, as each component represents one direction of the same measured force. Instead, we adopted a more intuitive approach by treating the three components as a single multidimensional curve and applying elastic shape alignment to obtain a common set of warping functions. This approach allows us to focus on the phase aspects shared by all three components. Note that the Fisher-Rao mathematics extend to multi-dimensional functions (Srivastava and Klassen, 2016), where the SRVF for a vector-valued function $f(t)$ becomes:

$$q(t) = \frac{\dot{f}(t)}{\sqrt{\|\dot{f}(t)\|}}.$$

A subset of GRF curves exhibited atypical vGRF or apGRF components, which posed challenges to aligning these curves with the rest of the data. Those GRFs were atypical in the sense that the vertical component lacked the two-peak structure expected of normal gait and appeared closer to unimodal, and/or the anterior-posterior component was close to zero and relatively flat. Examples of these atypical cases are highlighted in Figure 2,

with representative atypical cases colored by walking speed and other curves in gray. Each panel in this row corresponds to one component of the original (unaligned) GRF curves.

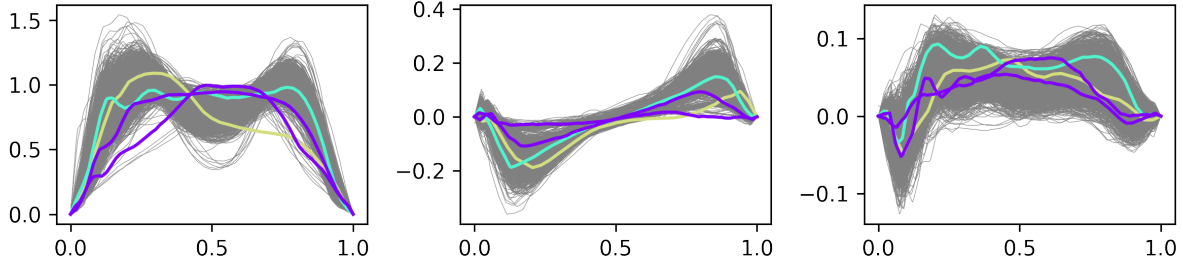


Figure 2: Left to right panels: vGRF, apGRF, and mlGRF curves. Examples of atypical GRF curves are highlighted, with representative atypical cases colored by walking speed and other curves in gray. These atypical curves lack the expected two-peak vertical structure or have near-zero, flat anterior-posterior components.

To address the lack of a common underlying structure, we registered the full dataset using the penalized elastic shape analysis procedure. By adjusting the elasticity parameter λ , we aligned the full set of GRF curves without distorting the shape of the atypical curves. To determine an appropriate λ , we computed warping functions iteratively over a grid of candidate values and visually examined the alignment results, focusing particularly on atypical curves. We refined the grid in regions where λ values produced reasonable results, selecting values that avoided excessive smoothing of features in the atypical curves while still capturing meaningful phase variation. Over-alignment led to sharp corners forming a staircase-like pattern in the warping functions, indicating drastic stretching and compression of curves with differing underlying structures, such as unimodal curves.

Based on this evaluation, we selected $\lambda = 2$ as a reasonable balance between alignment and over-alignment. To illustrate this trade-off, Figure 3 compares results for three λ values: the fully elastic case $\lambda = 0$ in the top row, our selected $\lambda = 2$ in the middle row, and a less elastic case $\lambda = 4$ in the bottom row. Atypical cases are colored by speed, while

other curves are shown in gray, as in Figure 2. The leftmost panels display the warping functions for each λ , where $\lambda = 0$ results in sharp staircase-like patterns indicative of over-alignment, while $\lambda = 4$ yields warping functions tightly clustered around the identity, suggesting insufficient alignment. The second through fourth columns show the aligned curves. Results for additional values of λ can be found in Figure 11 of the supplementary material.

While our approach treated alignment as agnostic to a specific performance criterion, a more formal selection method could be employed depending on the analytical objectives. For instance, if alignment quality is evaluated based on a predictive or inferential task, λ could be optimized via cross-validation to maximize a relevant performance metric. However, in finite samples, cross-validation may yield a noisy selection due to its slow convergence to optimal results (see [Hall and Marron \(1987\)](#) in the context of bandwidth selection for kernel density estimation). Alternatively, if the goal is to estimate an underlying common signal, [Kim et al. \(2023\)](#) provides a scale-space approach for estimating both the shape of the unknown signal and the signal itself. Defining a notion of optimality depends on the specific context of the analysis, and the choice of λ for different analytical objectives remains an open area of research.

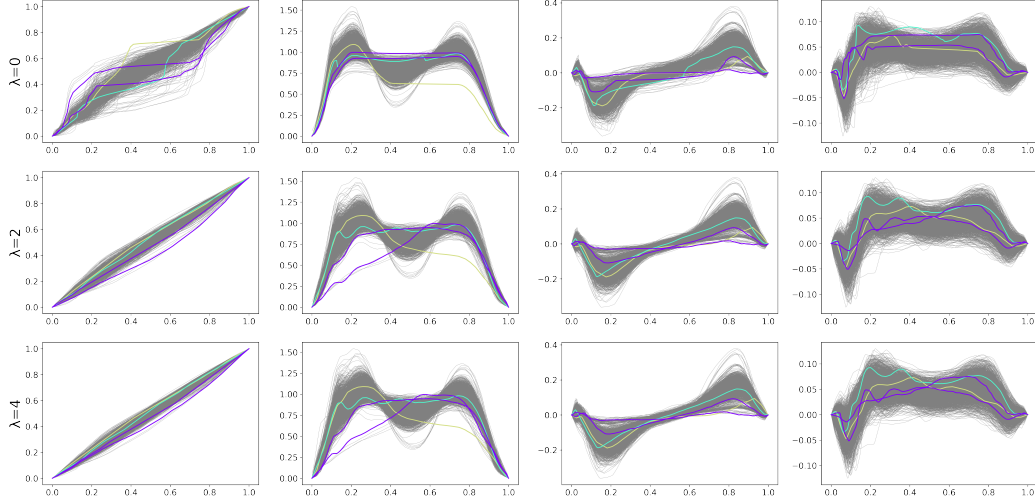


Figure 3: Alignment results for three elasticity parameter values: fully elastic ($\lambda = 0$), the selected $\lambda = 2$, and a more rigid case ($\lambda = 4$). Atypical cases are colored by speed, while other curves are shown in gray. The leftmost panels display the warping functions, and the second through fourth columns show the aligned curves. The staircasing effect in the fully elastic case ($\lambda = 0$) indicates over-alignment, while $\lambda = 4$ results in warping functions tightly clustered around the identity, suggesting insufficient alignment. The selected $\lambda = 2$ balances these effects.

Next, we obtained amplitude objects by applying the (common) set of warping functions to each set of original GRF curves, which gives an intuitive representation of each component’s amplitude. The amplitude objects obtained for different values of λ are shown in the second through fourth columns of Figure 3.

3.2 Modes of variation

In the OODA terminology, a collection of members of the object space that summarize one component of variation and is in some sense one-dimensional is called a *mode of variation*. For example, in the vector matrix case, a mode of variation is a rank-one matrix. We can obtain modes of variation through *Principal Component Analysis* (PCA), where each object is considered as a point in high dimensional space (column vector). For an introduction

to PCA, see Jolliffe (2002). For each direction of the ground reaction force (vGRF, apGRF, mlGRF), PCA was performed on the set of 2686 Fisher-Rao aligned curves, each corresponding to an individual gait observation, yielding the amplitude modes (Tucker et al., 2013). The sets of input curves are shown in the second, third, and fourth columns of the middle row of Figure 3.

Figure 4 shows the modes of variation of the amplitude objects of the vGRF, where the curves are colored according to walking speed. The first mode of variation, shown in the first panel of the second row of that figure, is associated with walking speed and reflects the contrast in peak heights and valley depths. Faster walkers (indicated in red in the rainbow color scheme) generally exhibit higher peaks and lower valleys, while slower walkers (purple in the rainbow color scheme) have lower peaks and a shallower valley. The middle column of that figure displays the largest (dashed curve) and smallest (dotted curve) PC projections added back to the mean curve, which is shown as a solid black curve in each of the middle panels. The middle panel of the first mode shows that the slowest walkers (dotted curve) exhibit a vertical amplitude force that appears unimodal and does not exceed body weight (1 on the vertical axis), indicating that these walkers do not fully transfer their weight to the striking limb. This type of gait can be thought of as “shuffling.” The second and third modes of variation are about the second and first peak, respectively. The middle panel in the third row shows the largest and smallest PC2 projections added back to the mean curve, distinguished with a dashed (largest) and dotted (smallest) line type. These extremes show that variation in this mode is mostly in the height of the second peak. In the panel below, the extremes of the third mode indicate phase variation in the first peak that is unique to the vertical component. The fourth mode of variation reflects the overall magnitude, particularly in the mid-stance phase. The second, third, and fourth PC projection extreme

curves all suggest that some curves have a small third bump before the first peak. In gait analysis, this pattern is known as the *heelstrike transient* (HST), a rapid and transient rise in the vGRF immediately after ground contact. As discussed in [Blackburn et al. \(2016\)](#) and references therein, the presence and characterization (e.g. magnitude) of HST indicate impulsive loading, which influences cartilage degradation and symptoms of OA. However, [Blackburn et al. \(2016\)](#) also noted that methods for identifying HST can be unreliable. The amplitude modes of variation we identified offer a potentially viable method for reliably identifying and understanding the HST.

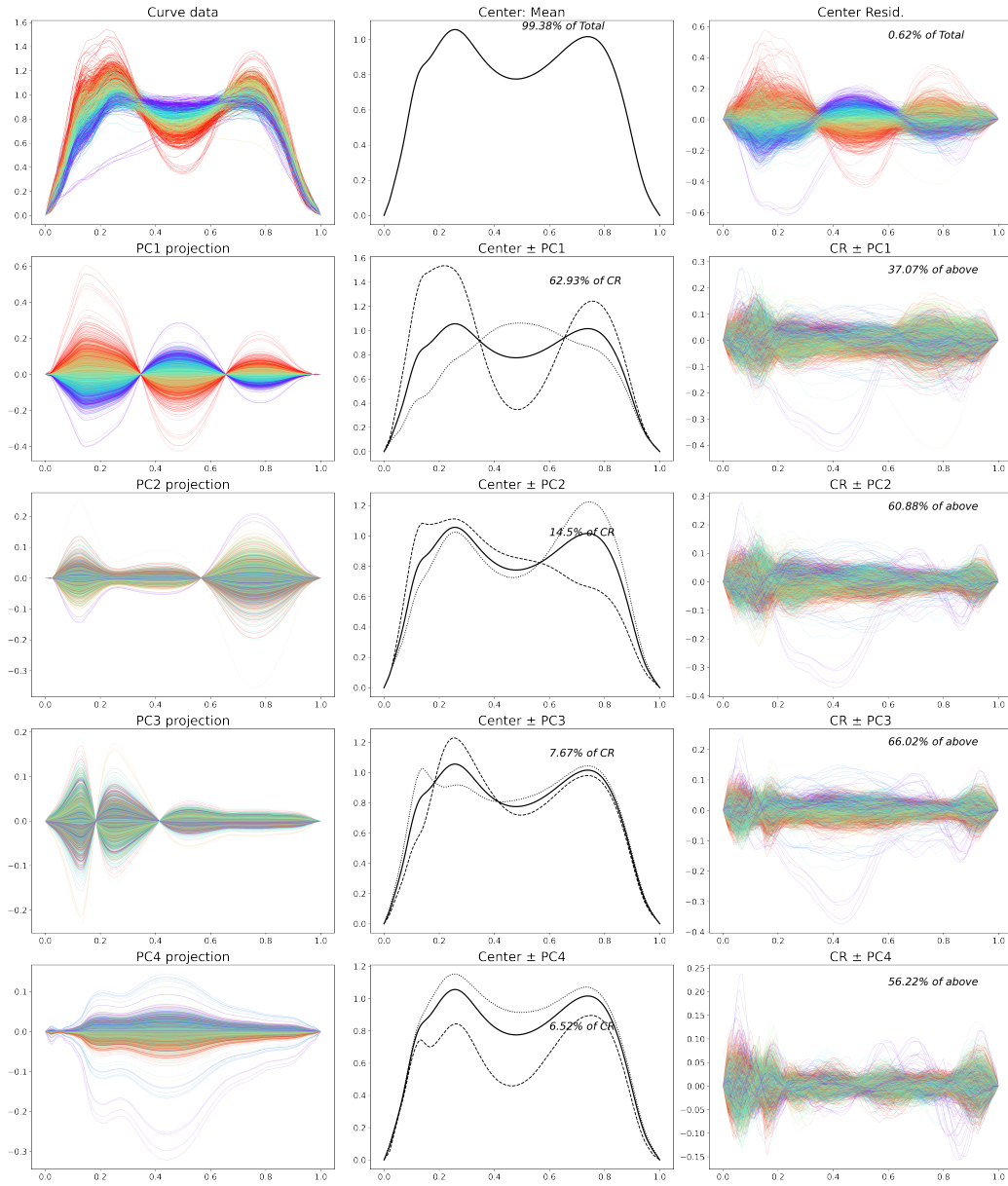


Figure 4: Modes of variation of the vGRF amplitude objects, shown in the top left panel. The first mode of amplitude variation, showing magnitude of the peaks and valley, is displayed in the second row, first panel. The panels in the middle column show the largest and smallest PC projections added back to the mean curve, while the solid black curve corresponds to the mean curve. The second and third modes of amplitude variation (third and fourth row, respectively) explain variation within each peak. The fourth mode indicates variation in overall magnitude, particularly of the valley, as seen in the middle panel of the last row.

Similar plots of the amplitude modes of variation of the components of apGRF and

mlGRF are provided in Section 2 in the supplementary material.

Extracting phase modes of variation requires more careful consideration. Recall from Section 3.1 that the warping functions all have corresponding SRVFs that lie on the surface of a high-dimensional sphere in the function space. Thus, using PCA to identify phase modes of variation is essentially an approximation in the tangent space centered on the Karcher mean. In the case of warping functions, these SRVFs must also lie on the positive orthant Wu et al. (2024). It is demonstrated in Yu et al. (2017) that in cases of high variation, this tangent plane PCA may yield a distorted analysis, resulting in modes of variation that leave the positive orthant and consequently produce invalid warping functions. This phenomenon was also observed in our dataset. In such scenarios, a better decomposition of the variation can be achieved using the functional PCA methodology proposed by Yu et al. (2017), which is based on an improved PCA analogue for spheres known as Principal Nested Spheres (PNS) proposed by Jung et al. (2012). The PNS decomposition sequentially provides the best k -dimensional approximation U^k of the data for all $k = d - 1, d - 2, \dots, 0$ such that

$$S^d \supset U_{d-1} \supset \dots \supset U_1 \supset U_0.$$

For each k , the sphere U^k , called the k -dimensional *principal nested sphere*, is a submanifold of the higher dimensional principal nested spheres. The algorithm to find sample principal nested spheres is determined by iteratively minimizing an objective function to find the best-fitting subsphere, projecting the data to the lower dimensional sphere, and mapping to the original space through a relevant transformation. The signed residuals, defined as the signed length of the minimal geodesic joining the (projected and transformed) data points to the subsphere, serve as analogs of principal component scores. Chapter 8 of Marron and Dryden (2021) provides further review of PNS and other geodesic-based methods.

We applied the PNS-based functional PCA methodology to the set of (common) warping functions to obtain phase modes of variation. We found that the great sphere decomposition from PNS yielded the most interpretable phase modes of variation because of weak interpretability of small sphere variation. Figure 5 depicts an intuitively useful notion of phase variation represented by warpings of the Karcher mean of the vGRF curves. The warping functions used to create these visualizations were generated by taking the inverse of the phase PNS projections added to the 45-degree line (identity warp). In each panel of the figure, the curves are colored based on the PNS scores for the corresponding mode, with cyan indicating the lowest scores and magenta indicating the highest. It is important to note that the curves are plotted in the order of the corresponding score, as over-plotting is an issue. The first mode (first panel) shows an overall shift in timing, with most apparent differences in the timing of the first peak (maximum heel-strike force) and valley. The second mode in the next panel appears to explain variability in the closeness of the peaks - the cyan curves are the curves with peaks closer together and the magenta curves have peaks farther apart. The third mode represents an overall phase shift (left vs. right) and seems to suggest that curves having a small third bump before the first peak correspond with an earlier timing (cyan curves), especially an earlier second peak. The fourth mode appears to highlight variability in the timing of the second peak, independent of the rest of the curve.

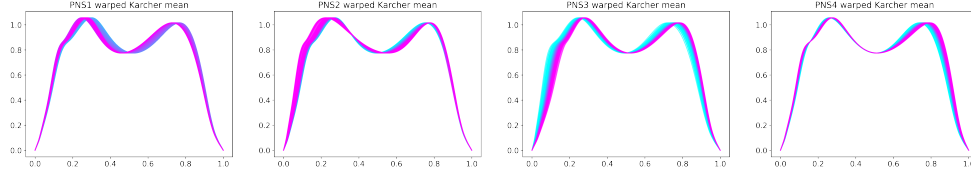


Figure 5: Visual representation of phase variation using warpings of the Karcher mean of the vGRF curves. Warping functions were generated by taking the inverse of the phase PNS projections added to the 45-degree line. Each panel shows curves colored by corresponding PNS scores, with cyan indicating the lowest scores and magenta indicating the highest. Curves are plotted in the order of the corresponding score to avoid over-plotting. The first panel (first mode) shows an overall shift in timing, with most apparent differences in the timing of the first peak (maximum heel-strike force) and valley. The second panel (second mode) shows variability in the closeness of the peaks. The third panel (third mode) represents an overall phase shift, suggesting earlier timing for curves with a small third bump before the first peak (cyan). The fourth panel (fourth mode) emphasizes variability in the timing of the second peak, independent of the rest of the curve.

4 Comparison to conventional discrete summaries

We investigated the added value of analyzing patterns across the entire movement curve, as opposed to conventional discrete summaries of GRF curves. To assess this, we compared the predictive performance of predictors derived from our shape-based analysis of the full movement curves with conventional discrete summaries in predicting disease severity.

Osteoarthritis (OA) severity is a critical outcome in disease treatment studies and is commonly evaluated using joint space width (JSW) measurements, as well as the Kellgren-Lawrence grade (KLG), a radiographic classification system, and patient-reported pain and function scores from the Western Ontario and McMaster Universities Arthritis Index (WOMAC) (Alexandersen et al., 2014). JSW, measured in millimeters on radiographic images, is particularly important for diagnosing and monitoring knee OA.

In the IDEA study, JSW was available for only a subset of patients. Therefore, we analyze it separately in this section, while analyzing other OA measures with larger sample sizes in the following section. While JSW narrowing is a key marker of disease progression, prior studies suggest that knees at similar stages of OA tend to progress at comparable rates (Benichou et al., 2010). Consequently, baseline JSW may provide a more meaningful indicator of disease severity than JSW change over time. Furthermore, because the IDEA study is a clinical trial of interventions for patients already having an advanced stage of knee OA, focusing on baseline measures is the most appropriate approach for this dataset. Given these considerations, we used baseline JSW as a dependent variable to compare full-curve predictors with conventional discrete summary predictors.

Baseline JSW measurements were missing for 129 out of the 454 IDEA participants. The missing values for JSW are shown in the last column of the heatmap in Figure 15 in the supplementary material, with red lines indicating missing values. The rest of that figure is discussed in Section 4.2. The reasons for the missing values were not reported in the data, but a comparison of clinical data for participants with and without baseline JSW measurements showed no apparent sampling bias. This left a total of 325 participants with baseline JSW data for our analysis.

To create predictors derived from our full-curve analysis, we combined scores for 16 distinct modes of amplitude variation from three types of curve data objects (vGRFs, apGRFs, and mlGRFs) and phase variation. Each mode is represented by either a set of amplitude PC scores or PNS phase scores. Below are listed the 16 sets of scores that together formed our predictor variables:

- PC1-PC4 scores of the vGRFs amplitude data objects (studied in Figure 4);
- PC1-PC4 scores of the apGRFs amplitude data objects (studied in Figure 12 in the

supplementary material);

- PC1-PC4 scores of the mlGRFs amplitude data objects (studied in Figure 13 in the supplementary material);
- Great sphere PNS1-PNS4 scores of the common phase data object (studied in Figure 5).

We developed a set of predictors based on conventional discrete summaries of GRF curves found in the literature, including the first peak of the vGRF curve (maximum over 0 – 50% of the stance), the minimum value of the apGRF curve (minimum over 0 – 100% of the stance) and the maximum value of the apGRF curve (maximum over 0 – 100% of stance).

Using JSW as the dependent variable, we conducted a comparison of multiple linear regression models. We first used either our full-curve predictors or the set of conventional discrete summaries as predictor variables. Since we treat curves as data objects, we used all 2686 gait curves as individual observations, where each curve was represented either by its full-curve predictors or by its corresponding set of conventional discrete summary predictors. We adjusted our hypothesis testing inference to account for the dependence among curves from the same patient, as described in the next two paragraphs.

The model using full-curve predictors achieved a coefficient of determination $R^2 = 0.2$, whereas the model using conventional discrete summary predictors had a much smaller value of $R^2 = 0.024$. Although both R^2 values were small, the model using full-curve predictors demonstrated a substantially stronger association with JSW. Given that OA is a complex, multi-system disease influenced by metabolic, inflammatory, post-injury, and aging-related factors beyond biomechanics, modest R^2 values are expected and common in the field.

We assessed the significance of the R^2 values using a bootstrap-based F-test. Standard F-tests assume independent observations, which is violated in our dataset due to a clear dependence between the multiple gait curves per patient. To account for this, we implemented a bootstrap procedure in which patients were resampled with replacement, and all gait curves associated with a selected patient were included in the resampled dataset. For each of 1000 bootstrap resamples, we refit the models and computed the F-statistics, constructing null distributions for model fit. All other bootstrap analyses in this paper also used 1000 replications. The significance of each model’s R^2 value was then assessed by computing the proportion of bootstrap F-statistics greater than or equal to the observed F-statistic from the original data. This resampling approach reflects the natural dependence structure in the data, providing an appropriate null distribution for inference. The results of this bootstrapping procedure showed that the R^2 for the model with full-curve predictors was significantly different from zero (p-value 0.022), while the R^2 for the model with conventional discrete summary predictors was not significantly different from zero (p-value 0.22).

Considering the complexity of OA disease and that the R^2 measure may arbitrarily favor larger models, a more nuanced comparison is appropriate to confirm the value added by using full-curve predictors. With this motivation, we conducted F-tests for nested models via bootstrapping to provide a more robust comparison, detailed in the following section.

4.1 Nested model comparison

We assessed the value added by full-curve predictors over conventional discrete summaries by comparing nested linear regression models. Specifically, we evaluated whether full-curve predictors provided additional predictive value beyond conventional discrete summaries

using a bootstrap-based F-test approach.

To compare these models, we computed the F-ratio for two cases: (1) a full model containing both full-curve predictors and conventional discrete summaries versus a reduced model containing only the full-curve predictors, and (2) the same full model versus a reduced model containing only the conventional discrete summaries. The null hypothesis for this F-test states that the additional predictors in the full model have coefficients equal to zero, meaning they do not contribute additional explanatory power. Failing to reject the null hypothesis when the reduced model contains the full-curve predictors suggests that the conventional discrete summaries do not add predictive value beyond the full-curve predictors. Conversely, rejecting the null hypothesis when the reduced model contains the conventional discrete summaries indicates that the full-curve predictors offer additional predictive value not captured by conventional discrete summaries alone. Similar interpretations apply when reversing the roles of the full-curve and conventional discrete summaries.

As before, we used all 2686 gait curves as individual observations, representing each curve either by its full-curve predictors or its corresponding set of conventional discrete summary predictors. We again accounted for the dependence between observations using a patient-level bootstrap resampling procedure. We then fit the full and reduced models to each resampled dataset and computed the F-statistic, constructing a null distribution for model comparison.

The results showed that the reduced model with only full-curve predictors was not rejected at the 0.05 significance level (p-value 0.34), suggesting that the addition of conventional discrete summaries did not improve model performance, whereas the reduced model with only conventional discrete summary predictors was rejected (p-value 0.016), indicating that full-curve predictors provided additional predictive value beyond conventional discrete

summaries. This comparison highlights that full-curve predictors offer greater predictive performance and explain more variation in the important disease indicator, JSW.

As previously noted, JSW is just one measure of OA severity. In the next section, we examine the other key indicators - KLG and WOMAC pain and function scores - along with additional clinical measures relevant to OA. By analyzing these broader severity measures and clinical traits, we further assess the added value of full-curve predictors compared to conventional discrete summaries.

4.2 Predicting clinical traits

Various clinical traits relevant to patient health, OA severity, and pain/functionality were collected as part of the IDEA study. These included data from the participant level on sociodemographics, pain, mental and physical health, OA severity, and others. We used a subset of these clinical traits as dependent variables to compare full-curve predictors with conventional discrete summaries using the same nested model procedure as before. We selected 40 out of 72 clinical traits for analysis by excluding those that were redundant with other traits and those with a high number of missing values.

Figure 15 in the supplementary material shows a heat map of missing values after removing redundant traits, with blue lines indicating missing values for each clinical trait. The first 40 traits in that figure are the selected ones. Recall that the last column in that figure corresponds to JSW, which is analyzed separately in Sections 4 and 4.1. Since additional data are available for other clinical traits, we conducted the analysis of disease severity using JSW separately, as discussed in those sections. Since these other clinical traits had relatively few missing values, we imputed the remaining missing values using the mean value of each corresponding trait. Table 1 in the supplementary material provides an

overview of the selected clinical data, including abbreviated trait names, brief descriptions, and trait types.

For each additional clinical trait, we repeated our comparison of multiple linear regression models, with the trait as the dependent variable and all 2686 gait curves represented either by full-curve predictors or conventional discrete summaries as independent variables. We maintained a consistent modeling strategy across all traits without specifically adjusting for binary or ordinal response variables or potential multicollinearity. While multiple linear regression may be conservative in such cases, our goal was to assess the relative predictive value of full-curve versus conventional discrete summary predictors under a uniform framework rather than to maximize predictive power for any specific trait. When conducting inference for each trait model, we again accounted for the dependence between observations using a patient-level bootstrap resampling procedure.

Figure 6 presents a scatter plot in which each axis represents the R^2 value for models using the respective predictor sets. The R^2 values were not significantly different from zero for both models using full-curve predictors and those using conventional discrete summary predictors when predicting the following clinical traits: Positive affect, Negative affect, Life satisfaction, SF-36 Mental, Mini Mental State, Number of falls, Heart attack, Heart failure, Heart arrhythmia, Stroke, Hypertension, Cancer, Diabetes, Depression, Pacemaker, Marital status, Education, Alcohol use, and Smoking. These traits, represented by gray circles in the figure, include comorbidities, mental and physical health measures not necessarily related to OA, and sociodemographic variables unlikely to be directly linked to biomechanics.

In contrast, the R^2 values were significantly different from zero for both predictor sets when modeling traits more directly relevant to gait, including: Gait efficacy, Balance con-

fidence, Exercise adherence, Fitness satisfaction, WOMAC function, SF-36 Physical, Hip circumference, Walking speed, Walk distance, BMI, Fear of falling, Thinking about falling, and Male. These traits are represented by green stars in the figure.

Notably, several traits had an R^2 value significantly different from zero for models using full-curve predictors but not for models using conventional discrete summary predictors. These traits include: Worst knee KLG, WOMAC pain, Weight, Waist circumference, Age, CRP, IL-6, and Black. These variables are all potentially important in knee OA. In particular, Worst knee KLG and WOMAC pain represent two important measures of OA severity, as discussed earlier, while CRP and IL-6 are inflammatory biomarkers that may contribute to OA development and progression. These traits are represented by a green plus sign in the figure. Importantly, there were no traits for which models using conventional discrete summary predictors had an R^2 value significantly different from zero while models using full-curve predictors did not.

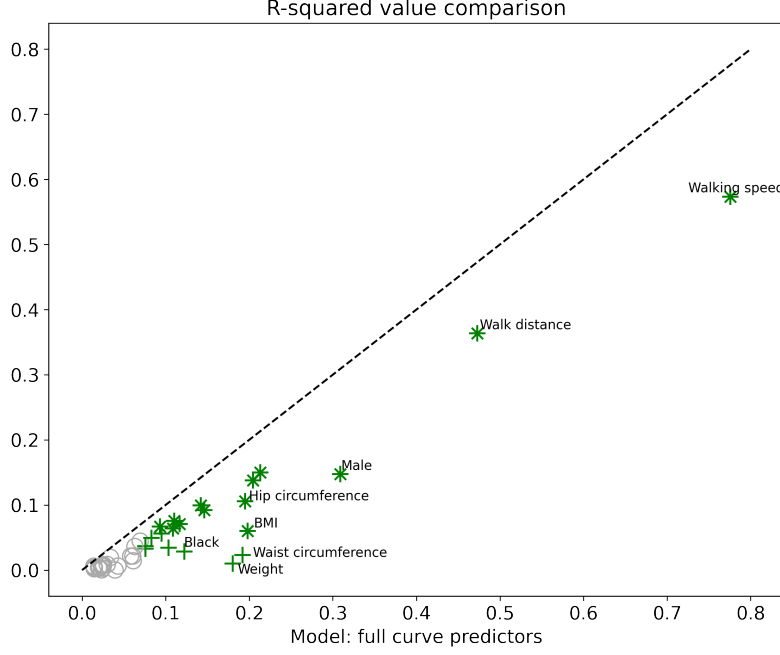


Figure 6: Scatter plot of R^2 values for models using full-curve predictors versus conventional discrete summaries. Gray circles indicate traits where R^2 was not significantly different from zero for either predictor set. Green stars mark traits where both models had significant R^2 values, while green plus signs indicate significance only for full-curve predictors. No traits showed significant R^2 values for conventional discrete summaries alone. All points fall below the diagonal ($x = y$), demonstrating consistently higher R^2 values for full-curve models. Points farther from the diagonal reflect greater differences, with the largest gaps observed for Walking speed, Walk distance, Male, Hip circumference, BMI, Waist circumference, Weight, and Black, which are labeled in the figure.

All points lie below the diagonal line ($x = y$), shown as a black dashed line in the figure, indicating that R^2 values for models based on full-curve predictors are consistently higher than those for conventional discrete summary predictors. The distance from the diagonal reflects the magnitude of this difference, with points farther from the line representing greater improvements in predictive performance when using full-curve predictors. As labeled in the figure, the largest differences in R^2 values were observed for models pre-

dicting Walking speed, Walk distance, Male, Hip circumference, BMI, Waist circumference, Weight, and Black.

Despite generally low R^2 values for both predictor sets, full-curve predictors consistently explain more variation in clinical traits, indicating that they capture more information than conventional discrete summaries.

4.3 Nested model comparison for predicting clinical traits

A nested model comparison again provided further insight into the added value of full-curve predictors. We computed the F-ratio for a full model containing both full-curve and conventional discrete summary predictors versus reduced models containing only one predictor set. We then generated a null distribution for the F-tests via patient-level bootstrapping and performed the inference as described previously. When no bootstrap replications were larger than the original statistic, we defined the p-value to be $\frac{1}{2*1000} = 0.0005$.

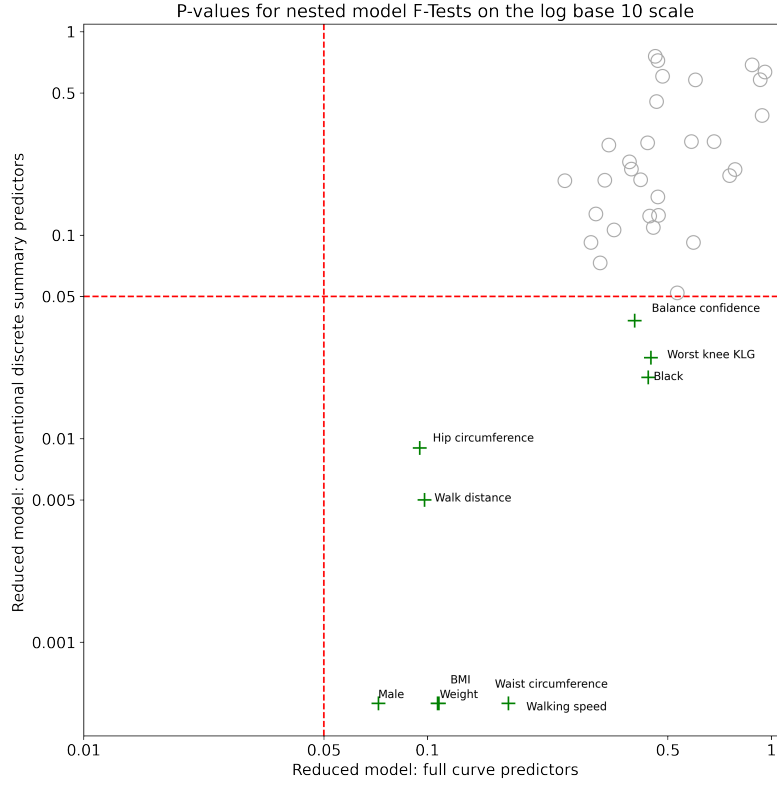


Figure 7: Scatter plot of bootstrap p-values resulting from F-tests of nested models, shown on a logarithmic scale. The horizontal axis represents the p-values for testing reduced models with full-curve predictors, and the vertical axis represents those for testing reduced models with conventional discrete summary predictors. For readability, the axes are labeled on the original scale. A red dashed line marks the $\log_{10}(0.05)$ threshold on both axes, corresponding to the 0.05 significance level. Gray circles represent traits where neither reduced model was rejected at this significance level, indicating that neither predictor set adds substantial predictive value. Green plus signs represent traits where the reduced model with full-curve predictors was not rejected, but the reduced model with conventional discrete summary predictors was rejected, highlighting the added value of full-curve predictors. No points appear to the left of the vertical red dashed line, indicating that the reduced model with full-curve predictors was never rejected and is consistently a suitable approach.

Figure 7 presents a scatterplot of p-values from F-tests of nested models, displayed on a base-10 logarithmic scale. The horizontal axis shows p-values for testing reduced models with full-curve predictors, while the vertical axis represents p-values for reduced models

with conventional discrete summary predictors. For readability, the axes are labeled on the original scale.

A red dashed line marks the $\log_{10}(0.05)$ threshold on both axes, corresponding to the 0.05 significance level. Gray circles represent models where neither reduced model was rejected, a category that includes most clinical traits. This is unsurprising, as many clinical traits have limited association with biomechanics or are inherently difficult to predict, meaning that more complex gait predictors would not be expected to provide much additional value beyond simpler models.

Green plus signs highlight models where the reduced model with full-curve predictors was not rejected, while the reduced model with conventional discrete summary predictors was rejected, meaning conventional summaries provided no additional predictive value. The corresponding traits include Worst knee KLG, Balance confidence, Weight, Waist circumference, Hip circumference, Walking speed, Walk distance, BMI, Male, and Black. These results are consistent with our previous R^2 comparisons, as these traits were either those for which only full-curve models had significant R^2 values or those where the R^2 values were substantially larger than those of models using conventional discrete summaries.

Importantly, there are no cases where the model with full-curve predictors is rejected while the model with conventional discrete summary predictors is not. In fact, no points appear to the left of the vertical red dashed line, indicating that the reduced model with full-curve predictors was never rejected and is consistently a suitable approach.

5 Conclusion

This paper quantitatively compares the information contained in the data objects of the complete GRF curve versus conventional discrete summaries on disease severity and clin-

ical profiles of patients with OA, demonstrating the greater value of analyzing the full curves. We apply a straightforward nested model comparison to highlight this difference. Furthermore, our shape-based approach offers an intuitive representation of full movement curves, applicable in broader analyses, and reveals insightful modes of variation. Our work is among the first to demonstrate the superior predictive potential of full movement curves over conventional discrete summaries and to compare these representations for predicting disease measures.

SUPPLEMENTARY MATERIAL

Supplement to Elastic Shape Analysis of Movement Data: Additional figures and tables, with accompanying brief discussions. (pdf)

Funding

The research reported in this paper was partially supported by the National Institutes of Health (NIH), including grants from the National Institute of Arthritis and Musculoskeletal and Skin Diseases (NIAMS) P30 AR072580 and K24 AR081368. Ashley N. Buck’s research was partially supported by NIAMS T32 AR082310. Additionally, the research of Jan Hannig and J. S. Marron was also partially supported by the National Science Foundation grant DMS-2113404. The IDEA study, from which the data presented in this paper was obtained, was supported in part by NIH grants R01 AR052528-01 from NIAMS, P30 AG21332 from the National Institute on Aging, and M01-RR00211 from the National Center for Research Resources, as well as by General Nutrition Centers.

References

- Alexandersen, P., Byrjalsen, I., Bay-Jensen, A.-C., Siebur, A.-S., Andersen, J., Riis, B., Christiansen, C. and Karsdal, M. (2014), ‘Association between joint space width, Kellgren-Lawrence score, pain and progression in osteoarthritis subjects from two phase III studies—a clinical study reference database’, *Osteoarthritis and Cartilage* **22**, S197. [21](#)
- Astephen, J. L., Deluzio, K. J., Caldwell, G. E. and Dunbar, M. J. (2008), ‘Biomechanical changes at the hip, knee, and ankle joints during gait are associated with knee osteoarthritis severity’, *Journal of orthopaedic research* **26**(3), 332–341. [2](#)
- Bauer, M., Charon, N., Klassen, E., Kurtek, S., Needham, T. and Pierron, T. (2024), ‘Elastic metrics on spaces of euclidean curves: Theory and algorithms’, *Journal of Nonlinear Science* **34**(3), 56. [11](#)
- Benichou, O., Hunter, D., Nelson, D., Guermazi, A., Kwok, K., Myers, S. and Duryea, J. (2010), ‘One-year change in radiographic joint space width in patients with unilateral joint space narrowing: data from the Osteoarthritis Initiative’, *Arthritis care & research* **62**(7), 924–931. [22](#)
- Bjornsen, E., Berkoff, D., Blackburn, J. T., Davis-Wilson, H., Evans-Pickett, A., Franz, J. R., Harkey, M. S., Horton, W. Z., Lisee, C., Luc-Harkey, B. et al. (2024), ‘Sustained limb-level loading: A ground reaction force phenotype common to individuals at high risk for and those with knee osteoarthritis’, *Arthritis & Rheumatology* . [3](#)
- Blackburn, J. T., Pietrosimone, B. G., Harkey, M. S., Luc, B. A. and Pamukoff, D. N. (2016), ‘Comparison of three methods for identifying the heelstrike transient during walking gait’, *Medical Engineering & Physics* **38**(6), 581–585. [17](#)

- Buck, A. N., Lisee, C. M., Bjornsen, E. S., Schwartz, T. A., Spang, J. T., Franz, J. R., Blackburn, J. T. and Pietrosimone, B. G. (2024), ‘Biomechanical threshold values for identifying clinically significant knee-related symptoms six months following anterior cruciate ligament reconstruction’, *Journal of Athletic Training* . **2**, **7**
- Costello, K. E., Felson, D. T., Neogi, T., Segal, N. A., Lewis, C. E., Gross, K. D., Nevitt, M. C., Lewis, C. L. and Kumar, D. (2021), ‘Ground reaction force patterns in knees with and without radiographic osteoarthritis and pain: descriptive analyses of a large cohort (the multicenter osteoarthritis study)’, *Osteoarthritis and cartilage* **29**(8), 1138–1146. **3**, **7**
- Davis, H. C., Luc-Harkey, B. A., Seeley, M. K., Blackburn, J. T. and Pietrosimone, B. (2019), ‘Sagittal plane walking biomechanics in individuals with knee osteoarthritis after quadriceps strengthening’, *Osteoarthritis and cartilage* **27**(5), 771–780. **3**
- Dillon, C. F., Rasch, E. K., Gu, Q. and Hirsch, R. (2006), ‘Prevalence of knee osteoarthritis in the United States: arthritis data from the Third National Health and Nutrition Examination Survey 1991-94.’, *The Journal of rheumatology* **33**(11), 2271–2279. **2**
- Dryden, I. L. and Mardia, K. V. (2016), *Statistical shape analysis: with applications in R*, Vol. 995, John Wiley & Sons. **2**
- Felson, D. T. (2013), ‘Osteoarthritis as a disease of mechanics’, *Osteoarthritis and cartilage* **21**(1), 10–15. **2**
- Guilak, F. (2011), ‘Biomechanical factors in osteoarthritis’, *Best practice & research Clinical rheumatology* **25**(6), 815–823. **2**

- Hall, P. and Marron, J. (1987), ‘On the amount of noise inherent in bandwidth selection for a kernel density estimator’, *The Annals of Statistics* pp. 163–181. [14](#)
- Hebenstreit, F., Leibold, A., Krinner, S., Welsch, G., Lochmann, M. and Eskofier, B. M. (2015), ‘Effect of walking speed on gait sub phase durations’, *Human movement science* **43**, 118–124. [5](#)
- Helwig, N. E., Hong, S., Hsiao-Wecksler, E. T. and Polk, J. D. (2011), ‘Methods to temporally align gait cycle data’, *Journal of biomechanics* **44**(3), 561–566. [5](#), [8](#)
- Hunt, M. A., Birmingham, T. B., Giffin, J. R. and Jenkyn, T. R. (2006), ‘Associations among knee adduction moment, frontal plane ground reaction force, and lever arm during walking in patients with knee osteoarthritis’, *Journal of biomechanics* **39**(12), 2213–2220. [7](#)
- Jolliffe, I. T. (2002), *Principal component analysis*, Springer Series in Statistics, second edn, Springer-Verlag, New York. [16](#)
- Jordan, J. M., Helmick, C. G., Renner, J. B., Luta, G., Dragomir, A. D., Woodard, J., Fang, F., Schwartz, T. A., Abbate, L. M., Callahan, L. F. et al. (2007), ‘Prevalence of knee symptoms and radiographic and symptomatic knee osteoarthritis in African Americans and Caucasians: the Johnston County Osteoarthritis Project.’, *The Journal of rheumatology* **34**(1), 172–180. [2](#)
- Jung, S., Dryden, I. L. and Marron, J. S. (2012), ‘Analysis of principal nested spheres’, *Biometrika* **99**(3), 551–568.
- URL:** <https://doi.org/10.1093/biomet/ass022> [19](#)

- Kim, W. M., Dasgupta, S. and Srivastava, A. (2023), ‘Peak-persistence diagrams for estimating shapes and functions from noisy data’, *arXiv preprint arXiv:2305.04826* . **14**
- Lawrence, R. C., Felson, D. T., Helmick, C. G., Arnold, L. M., Choi, H., Deyo, R. A., Gabriel, S., Hirsch, R., Hochberg, M. C., Hunder, G. G. et al. (2008), ‘Estimates of the prevalence of arthritis and other rheumatic conditions in the United States: Part II’, *Arthritis & Rheumatism* **58**(1), 26–35. **2**
- Marron, J. and Dryden, I. L. (2021), *Objected Oriented Data Analysis*, Chapman and Hall/CRC. **3, 8, 11, 19**
- Marron, J. S., Ramsay, J. O., Sangalli, L. M. and Srivastava, A. (2015), ‘Functional data analysis of amplitude and phase variation’, *Statistical Science* pp. 468–484. **9**
- Messier, S., Legault, C., Mihalko, S., Miller, G., Loeser, R., DeVita, P., Lyles, M., Eckstein, F., Hunter, D., Williamson, J. and Nicklas, B. (2009), ‘The intensive diet and exercise for arthritis (idea) trial: Design and rationale’, *BMC musculoskeletal disorders* **10**, 93. **1, 3**
- Messier, S., Mihalko, S., Legault, C., Miller, G., Nicklas, B., DeVita, P., Beavers, D., Hunter, D., Lyles, M., Eckstein, F., Williamson, J., Carr, J., Guermazi, A. and Loeser, R. (2013), ‘Effects of intensive diet and exercise on knee joint loads, inflammation, and clinical outcomes among overweight and obese adults with knee osteoarthritis the idea randomized clinical trial’, *JAMA : the journal of the American Medical Association* **310**, 1263–73. **1, 3**
- Messier, S. P., Loeser, R. F., Hoover, J. L., Semble, E. L. and Wise, C. M. (1992), ‘Osteoarthritis of the knee: effects on gait, strength, and flexibility’, *Archives of physical medicine and rehabilitation* **73**(1), 29–36. **7**

- Muniz, A. M. S., Manfio, E. F., Andrade, M. C. and Nadal, J. (2006), Principal component analysis of vertical ground reaction force: A powerful method to discriminate normal and abnormal gait and assess treatment, *in* ‘2006 International Conference of the IEEE Engineering in Medicine and Biology Society’, pp. 2683–2686. [3](#)
- Sims, E. L., Carland, J. M., Keefe, F. J., Kraus, V. B., Guilak, F. and Schmitt, D. (2009), ‘Sex differences in biomechanics associated with knee osteoarthritis’, *Journal of women & aging* **21**(3), 159–170. [2](#)
- Srivastava, A. and Klassen, E. (2016), *Functional and Shape Data Analysis*, Springer. [12](#)
- Srivastava, A., Wu, W., Kurtek, S., Klassen, E. and Marron, J. S. (2011), ‘Registration of Functional Data Using Fisher-Rao Metric’, *arXiv preprint arXiv: 1103.3817*. [9](#), [10](#)
- Trentadue, T. P. and Schmitt, D. (2024), ‘Fourier analysis of the vertical ground reaction force during walking: Applications for quantifying differences in gait strategies’, *Journal of Applied Biomechanics* **1**(aop), 1–9. [3](#)
- Tucker, J. D., Wu, W. and Srivastava, A. (2013), ‘Generative models for functional data using phase and amplitude separation’, *Computational Statistics and Data Analysis* **61**, 50–66. [9](#), [12](#), [16](#)
- Vos, T., Flaxman, A. D., Naghavi, M., Lozano, R., Michaud, C., Ezzati, M., Shibuya, K., Salomon, J. A., Abdalla, S., Aboyans, V. et al. (2012), ‘Years lived with disability (YLDs) for 1160 sequelae of 289 diseases and injuries 1990-2010: a systematic analysis for the Global Burden of Disease Study 2010’, *Lancet (London, England)* **380**(9859), 2163. [2](#)
- Wiik, A. V., Aqil, A., Brevadt, M., Jones, G. and Cobb, J. (2017), ‘Abnormal ground

- reaction forces lead to a general decline in gait speed in knee osteoarthritis patients’, *World journal of orthopedics* **8**(4), 322. [7](#)
- Wu, W. and Srivastava, A. (2011), ‘An information-geometric framework for statistical inferences in the neural spike train space’, *Journal of Computational Neuroscience* **31**, 725–748. [11](#)
- Wu, Y., Huang, C. and Srivastava, A. (2024), ‘Shape-based functional data analysis’, *TEST* **33**(1), 1–47. [10](#), [19](#)
- Xiang, S. (2023), Binary Expansion Testing and Gait Force Analysis, PhD thesis, University of North Carolina at Chapel Hill. [12](#)
- Younes, L. (1998), ‘Computable elastic distances between shapes’, *SIAM Journal on Applied Mathematics* **58**(2), 565–586. [9](#)
- Yu, Q., Lu, X. and Marron, J. (2017), ‘Principal nested spheres for time-warped functional data analysis’, *Journal of Computational and Graphical Statistics* **26**(1), 144–151. [19](#)
- Zeni Jr, J. A. and Higginson, J. S. (2009), ‘Differences in gait parameters between healthy subjects and persons with moderate and severe knee osteoarthritis: a result of altered walking speed?’, *Clinical biomechanics* **24**(4), 372–378. [7](#)
- Zhang, Y. and Jordan, J. M. (2010), ‘Epidemiology of osteoarthritis’, *Clinics in geriatric medicine* **26**(3), 355–369. [2](#)